Optimisation and validation of a co-manipulated robot for brachytherapy procedure

Aziza Ben Halima, Julien Bert, Jean-françois Clément, Dimitris Visvikis

Received: 22 February 2022 | Revised: 25 August 2022 | Accepted: 27 September 2022

DOI: 10.1002/rcs.2465

ORIGINAL ARTICLE

The International Journal of Medical Robotics and Computer Assisted Surgery

WILEY

Optimisation and validation of a co-manipulated robot for brachytherapy procedure

Aziza Ben Halima | Julien Bert | Jean-François Clément | Dimitris Visvikis

Laboratory of Medical Image Processing (LaTIM), INSERM UMR 1011, University of Western Brittany (UBO), Brest, France

Correspondence
Julien Bert, Laboratory of Medical Image Processing (LaTIM), INSERM UMR 1011, University of Western Brittany (UBO), Brest 29200, France.
Email: julien.bert@univ-brest.fr

Abstract

Background: Low-dose rate brachytherapy is the referent treatment for early-stage prostate cancer and consists in manually inserting radioactive seeds within the organ to destroy tumorous cells. This treatment is inaccurate leading to side effects. Researchers developed robots to improve this technique. Despite ameliorating accuracy, they cannot be clinically used because of size and acceptability. Therefore, a 6-DOF parallel and co-manipulated robot is proposed to meet these requirements.

Methods: To fulfil the application requirements, a compact design was modelled. The robot's optimal dimensions were defined by establishing kinematics and implementing genetic algorithm. The robot's relevance was evaluated by measuring workspace and needle placement errors.

Results: The robot fits into a cube of $300 \times 300 \times 300$ mm^3 and provides a free-singularity workspace of $55 \times 55 \times 150$ mm^3 with a possible end-effector rotation of 15° and a needle placement error <3 mm.

Conclusion: The results are promising and prove that our robot fulfils the application requirements and presents a beneficial alternative to the manual procedure.

KEYWORDS
co-manipulation, medical robotics, prostate brachytherapy

1 | INTRODUCTION

Low-dose rate (LDR) brachytherapy is the referent treatment with the fewest long-term side effects of early-stage prostate cancer.[1] It has been proved to be very effective and safe, providing a good alternative to surgical removal of the prostate due to the targeted delivery of radioactive seeds, most commonly Iodine 125 (^{125}I), inside the organ to destroy the tumour cells while reducing the risk of unnecessary damage of healthy nearby tissues. Low-dose rate brachytherapy is usually an outpatient surgery and it is done over several steps. Before the establishment of the treatment plan in order to determine the target positions of radioactive seed placement, the anesthetized patient is installed on the operating table in a lithotomy position and the needle insertion assistance system, composed principally of a holed grid template, a stepper and an ultrasound probe, is set up. Then, the surgeon inserts 18 G needles via the transperineal surface across the fixed grid holes until reaching the prostate. He releases about 60–120 radioactive seeds along a straight trajectory under real-time ultrasound guidance. Finally, the needles are taken out leaving the permanent seeds behind to irradiate the tumorous cells. This internal radiotherapy provides a relatively short recovery time and minimises the toxicity of healthy tissues compared to other treatments like the external radiotherapy or the prostatectomy.[2] Despite the advantages of this localised

treatment in terms of efficacy and minimised toxicity, it has several limitations (difficulty of the procedure, 5 mm spacing grid template holes, depending on the surgeon's experience and dexterity, low-quality ultrasound images, etc.). These limitations cause inaccuracies in the manual placement of radioactive seeds in the prostate that can reach 6 mm.[3,4] The delivered dose is then slightly different that the one defined by the treatment planning.

Due to these inaccuracies this treatment sill lead some small side effects (urinary and sexual). In addition, such misplacement of the seeds limits the deployment of new protocol such focal therapy. This method consists of decreasing the side effects by treating only a small part of the prostate, where there is the tumour, instead of the whole gland as it is performed in the standard protocol. However, such focal therapy requires an accurate seed placement (~1 mm) in order to treat the cancer at the right position. The question here is how to improve the treatment delivery in order to have localised and focussed brachytherapy so that we can place the seed in the right place and have a final disposition identical to the treatment plan.

A robotic solution that guides the surgical gesture can be an alternative solution to overcome the drawbacks of the manual approach, improve the quality of care and provide a more precise and faster procedure. Recently, several researchers have been developing robotic systems for performing LDR brachytherapy. A complete review of image-guided robot for LDR brachytherapy is illustrated in the TG-192 report.[5] Some of these researchers tried to integrate industrial robots in the operating room like in Ref. 6. Other researchers developed serial robots dedicated to LDR brachytherpy as in Refs. 7–9. Parallel robots were also used to place radioactive seeds into the prostate such as in Refs. 10 and 11. These different systems showed the feasibility of robotising the manual procedure and were successfully tested on phantoms. Preliminary results show that the accuracy in placing brachytherapy needles is <3 mm.[12] Even though the results obtained are not yet sufficient, they are promising and validate the importance of using a robot during LDR brachytherapy. However, these robots have several issues that limit their deployment in the operating room. The first one is the size seeing that the majority of robots are heavy, bulky and cannot be easily deployed in the operating room. The second problem is the acceptability by surgeons to use robots since they are designed primarily for automatic or semi-automatic seed placement. Therefore, the major challenge is to propose a robot which, on the one hand, improves the surgical gesture, and on the other hand, try to resolve the issues of the existing medical robots for LDR brachytherapy.

In our previous work,[13] considering that parallel robots are more compact and precise than the serial robot, we propose to use a parallel (3-DOF) system for the robot in order to solve the problems of cumbersomeness and bulkiness and ensure easy and quick installation on the operating table under the patient's legs. The proposed design was also though, as a collaborative robot to ensure co-manipulation with the surgeon. The robot and the surgeon will work together, that is, the robot will help the surgeon to place seed, but the surgeon will keep control over the insertion of the needles. This should help the acceptability of the robotised solution by the surgeons. A simple proof of concept of this system was realised and results have shown that 3-DOF is not sufficient for the medical application, where oriented trajectories are essential to place the needle and seed properly within the prostate.[14] In addition, a lack of accuracy was observed due to the weight of the robot arms. We resolve this issue by theoretically designing a 6-DOF robot and proposing a gravity compensation system for such parallel robot in Ref. 15.

In this paper, our objective was to evaluate the adequacy of the 6-DOF robotic system to meet the requirements of the medical application. We present how the dimensions of this new design were optimised in order to ensure a compromise between a compact size and a sufficient workspace. The accuracy of the needle's tip placements was also evaluated with preliminary experimental results.

2 | ROBOTIC SYSTEM REQUIREMENTS

It is crucial to determine the different technical and clinical specifications that a robot for LDR brachytherapy must guarantee. The following design requirements were fixed depending on the constraints of the medical application, the literature review and the return of clinicians familiar with ultrasound guided prostate interventions.

- The system overall dimensions must fit into a cube of a volume of $300 \times 300 \times 300$ mm^3 to facilitate its installation in the limited workspace constrained by the ultrasound probe and the legs of the patient who is in a lithotomy position. The robotic structure should be set in front of the perineal surface and have to be adapted to be fixed on the operating table.
- A free-singularity translation workspace defined as a volume of $55 \times 55 \times 150$ mm^3 is required for the robot to attend any target position in the prostate. This requirement is defined based on the average dimension of an adult prostate that is approximately contained in a box of $40 \times 40 \times 40$ mm^3 and the width can attend 50 mm for the cases of enlarged prostate.[16] The distances between the rectal wall and the prostate capsule at the base and the apex are respectively 95 and 72 mm.[17]
- A needle rotation of 15° is needed for the yaw and pitch angle to minimise seed misplacement errors and avoid the interference with the pubic arch.[18] A needle rotation around its axis is privileged to compensate tissue deformations and prostate rotation due to the forces of insertion (see Figure 2 to identify pitch and yaw angles).

3 | MECHANICAL DESIGN

Inspired by the parallel 6-RUS manipulator proposed by,[19] we designed a robotic structure composed of two platforms. The first platform (fixed platform on Figure 1) will be fixed to the operating table parallel to the perineal surface and allows access to the

patient's perineum. The second one (end-effector on Figure 1) is mobile and it plays the role of the end-effector that holds the needle and will be co-manipulated by the surgeon. The design of the end-effector was adapted to ensure a secure fixation and ease release of the needle by clinicians. Also, it was parameterised to allow an ergonomic grip by the surgeons. These two platforms are linked by six kinematic chains: each one contains an active pivoting link motorized by six actuators that will be installed on the fixed platform, a passive universal joint and a passive spherical link (see our CAD model presented by Figure 1). A more detailed description on the adaptation of the 6-RUS manipulator to get our proposed robotic structure is illustrated in Ref. 15.

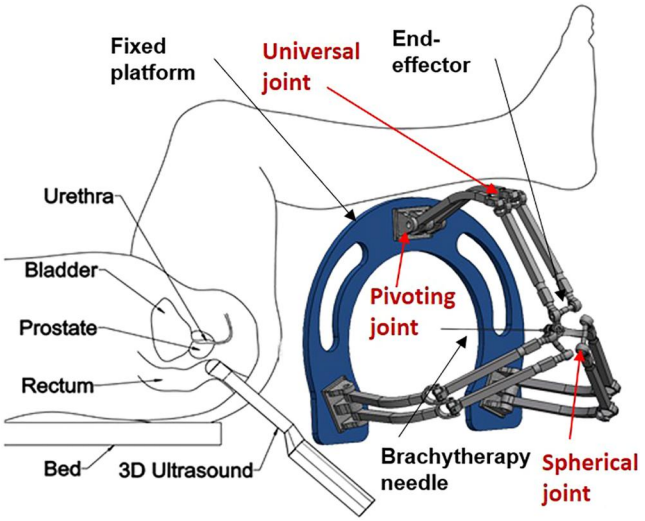

FIGURE 1 Schematic description of the proposed robotic structure in place during the low-dose rate brachytherapy

4 | KINEMATICS OF THE ROBOT

4.1 | Nomenclature of the robot

The following notations are used to describe the nomenclature of the robot mentioned in Figure 2 and that will be employed to solve the kinematics.

- The fixed coordinate system $R_0 = (O, x_0, y_0, z_0)^T$, of origin O placed at the centre of gravity of the base, is defined relative to the fixed platform.
- The end-effector coordinates system $R = (P,x,y,z)^T$, of origin P placed at the centre of gravity of the end-effector, is defined relative to the robot's end-effector.
- The coordinate system $R_i = (A_i, x_i, y_i, z_i)^T$ is defined relative to the pivoting joint of the ith kinematic chain that is attached to the fixed platform, $\forall i \in$.[1,6]
- $\mathbf{X} = [x, y, z, \alpha, \beta, \gamma]$ is the pose of the end-effector defined in P relatively to R_0.
- A_i, B_i and C_i are respectively centre of the ith pivoting joint, centre of the ith universal joint between the ith lower and top frames and centre of the ith spherical joint, $\forall i \in$.[1,6]
- r and R are respectively the radius of the fixed platform and the end-effector.
- $L_1 = \|B_i - A_i\|$ and $L_2 = \|C_i - B_i\|$ are respectively the length of the lower and top frames.
- θ_c and θ_A are respectively the angles between the neighbouring joints on the fixed platform and the end-effector.
- θ_d defines how to place two arms beside each other, it presents the angle between OA_i and the image of C_iB_i on the fixed platform, $\forall i \in$.[1,6]

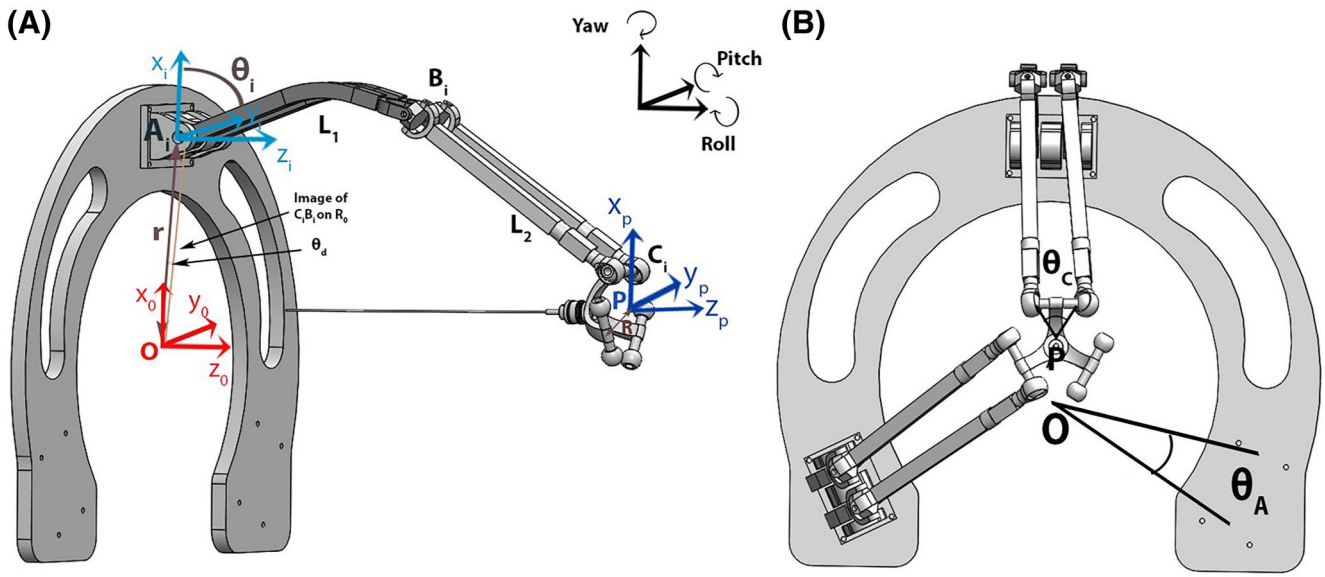

FIGURE 2 Robot nomenclature representing the geometric parameters and the different coordinate systems used to get the kinematics of the robot: (A) front view, (B) left view

- θ_i is the angle of the actuated pivoting joint, $\forall i \in$.[1,6] $\boldsymbol{\Theta} = [\theta_1, \theta_2, \theta_3, \theta_4, \theta_5, \theta_6]^T$ is the vector of the actuated pivoting joints.

4.2 | Inverse geometric model

It defines the relation between the pose of the end-effector and the pivoting joint angles θ_i. According to Ref. 15, the inverse geometric model is expressed as follows:

$$\theta_i = 2.\arctan\left(\frac{V_i \pm \sqrt{V_i^2 - W_i^2 + U_i^2}}{U_i + W_i}\right) \quad (1)$$

with

$$U_i = C_{ix}.\cos(\theta_{d_i}) + C_{iy}.\sin(\theta_{d_i}) - r.\cos(\theta_{d_i} - \theta_{A_i}) \quad (2)$$

$$V_i = C_{iz} \quad (3)$$

$$W_i = \frac{(C_{ix} - r.\cos(\theta_{A_i}))^2 + (C_{iy} - r.\sin(\theta_{A_i}))^2 + C_{iz}^2 + L_1^2 - L_2^2}{2.L_1} \quad (4)$$

4.3 | Forward geometric model

It provides the pose of the end-effector $\mathbf{X}$ corresponding to $\boldsymbol{\Theta}$. The most efficient approach used to calculate forward geometric model of a 6-RUS parallel manipulator is the iterative Newton-Raphson numerical scheme. For that, we can use the inverse geometric model determined in the previous paragraph to compute a numerical solution of the forward geometric model in an iterative manner. Taking advantage from the relation $\boldsymbol{\Theta} = \mathbf{IGM}(\mathbf{X})$ with IGM is the inverse geometric model and the differential model $\delta\mathbf{X} = J^{-1}\delta\boldsymbol{\Theta}$ with J^{-1} is the Jacobian matrix of the robotic structure dedicated to LDR brachytherapy and it will be explained in details in the next paragraph. $\delta\mathbf{X}$ is an increment of the pose of the end-effector and $\delta\boldsymbol{\Theta}$ a small increment of the pivoting joint angles. The forward geometric model of the robot calculating the poses $\mathbf{X}$ corresponding to the active joint positions $\boldsymbol{\Theta}$ is determined according to the iterative algorithm detailed below:

- An initial location $\mathbf{X_0}$, randomly chosen or an estimation close to the current solution, is defined. Then, it will be introduced to the IGM to compute the corresponding actuating joint variables $\boldsymbol{\Theta_0}$.
- Calculation $\mathbf{X_{k+1}}$ at iteration $k + 1$ by the iterative scheme of the Newton-Raphson method defined as follows:

$$\mathbf{X_{k+1}} = \mathbf{X_k} + J^{-1}(\boldsymbol{\Theta}_k - \mathbf{IGM}(\mathbf{X_k})) \quad (5)$$

- Compute the difference between $\boldsymbol{\Theta}_k$ and $\mathbf{IGM}(\mathbf{X_k})$.
  If $|\boldsymbol{\Theta}_k - \mathbf{IGM}(\mathbf{X_k})| < \varepsilon$ where ε is a fixed threshold, then the iterative scheme stops. Otherwise, the current end-effector pose is updated using Equation (5).
- Return to the first step.

To verify the results, an algorithm with the calculation described above was established and verified with MATLAB. This algorithm considers the dimensions of the robot presented in Table 2 and the different positioning configurations of the needle introduced in Figure 3. Table 1 presents the error between the real position and the position obtained after the resolution of the forward robot geometric model by the Newton-Raphson method. The average error, for all the points studied, is 0.86 mm which is sufficient to validate this method of calculation given the complexity of resolution of the forward geometric model for the 6-RUS manipulators.

4.4 | Jacobian matrix of the robot

To find the Jacobian matrix, we know that:

$$\left([P + R_p.C_{i_R}] - [A_{i_{R_0}} + B_{i_{R_i}}]\right)^T \left([P + R_p.C_{i_R}] - [A_{i_{R_0}} + B_{i_{R_i}}]\right) = L_2^2 \quad (6)$$

By deriving the previous relation, we get:

$$\lambda_i^T.\dot{P} + \lambda_i^T.\dot{R}_p.C_{i_R} - \lambda_i^T.\dot{B_{iR_i}} = 0 \quad (7)$$

With:

$$\lambda_i = [P + R_p.C_{i_R}] - [A_{i_{R_0}} + B_{i_{R_i}}] \quad (8)$$

$$\dot{B_{iR_i}} = L_1.\dot{\theta}_i[-\sin(\theta_i).\cos(\theta_{d_i}), -\sin(\theta_i).\sin(\theta_{d_i}), \cos(\theta_i)]^T \quad (9)$$

TABLE 1 Error between the real position and the position obtained by the calculation of the forward geometric model for different needle positioning configurations

Points	A	B	C	D	E	F	G	H	I
Error (mm)	0.02	1.4	1	1	0	1.4	1	1	1

TABLE 2 Upper and lower limits of the vector δ and result of optimisation

	r (mm)	R (mm)	L_1 (mm)	L_2 (mm)	θ_A	θ_c	θ_d
Min	80	30	100	100	20°	20°	−10°
Max	150	40	250	250	60°	60°	180°
Found by the optimiser	90	30	120	137.5	30°	60°	0°

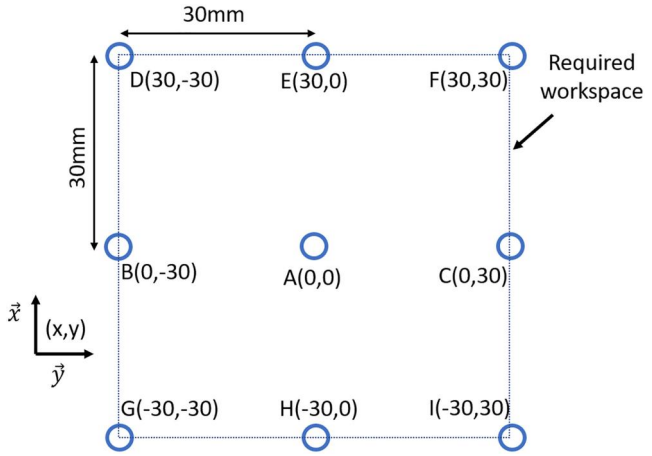

FIGURE 3 Identification of the positioning points of the needle

$$\dot{R}_p = \begin{bmatrix} 0 & -\dot{\alpha} & \dot{\beta} \\ \dot{\alpha} & 0 & \dot{\gamma} \\ -\dot{\beta} & \dot{\gamma} & 0 \end{bmatrix} R_p \tag{10}$$

By replacing these two previous parameters in Equation (7), we get:

$$\lambda_i^T.\dot{P} + \left(R_p.C_{i_R} \times \lambda_i\right)^T.\omega_p = \lambda_{q_i}.\dot{\theta}_i \tag{11}$$

with $\omega_p = (\dot{\alpha}, \dot{\beta}, \dot{\gamma})^T$ and

$$\lambda_{q_i} = \lambda_i^T.L_1\left[-\sin(\theta_i).\cos(\theta_{d_i}), -\sin(\theta_i).\sin(\theta_{d_i}), \cos(\theta_i)\right]^T \tag{12}$$

Finally, the relation between the velocity vector of the mobile platform and the one of the actuated pivoting joints is obtained when:

$$J_X.\left[\dot{P}, \omega_p\right]^T = J_q.\left[\dot{\theta}_1, \dot{\theta}_2, \dot{\theta}_3, \dot{\theta}_4, \dot{\theta}_5, \dot{\theta}_6\right]^T \tag{13}$$

with

$$J_X = [M_1, M_2, M_3, M_4, M_5, M_6, M_6]^T \tag{14}$$

$$M_i = \left[\lambda_i^T.\left(R_p.C_{i_R} \times \lambda_i\right)^T\right] \tag{15}$$

$$J_q = \begin{bmatrix} \lambda_{q_1} & & \\ & \ddots & \\ & & \lambda_{q_6} \end{bmatrix} \tag{16}$$

Then, the Jacobian matrix is expressed as following:

$$J = J_q^{-1}.J_X \tag{17}$$

4.5 | Singularities of the robot

According to Ref. 20, singularities occur when the Jacobian matrix becomes rank deficient. The 6-RUS parallel manipulator is composed of six spatial slider-crank mechanisms. By analogy with the planar slider–crank mechanism, singularities are detected when each rod of the universal joint and its corresponding crank lies in the same plane.[21] As a consequence, each actuator has two singularity positions. The first one occurs when the crank and the rod are nearly aligned, which corresponds to $[\det(J_q) = 0 \Leftrightarrow \theta_i = K\pi, \forall K \in \mathbb{Z}]$, and the second one when they are nearly superimposed, which corresponds to $\left[\det(J_x) = 0 \Leftrightarrow \theta_i = \frac{K\pi}{2}, \forall K \in \mathbb{Z}\right]$.

5 | OPTIMISATION OF THE DESIGN OF THE ROBOT

One of the major limitations of the 6-RUS manipulator is the restricted workspace of the end-effector. This disadvantage is related to the greater number of chains that link the base to the mobile platform and to the small range of movement of passive joints (spherical and universal joints). Thereby, the choice of the robot's geometrical parameters presents a relatively important step in proposing a compact robotic structure capable of being inserted into the available volume, limited by the patient's legs and the ultrasound probe, with a workspace that meets the requirements of the medical application.

The optimisation is a solution that has been adopted by researchers to guarantee performance criterion (control accuracy, speed, payload capability, stiffness, etc.) for parallel manipulators. Only a few researchers used it to find the optimal design of 6-RUS manipulator.[22–24]

In our study, we decided to apply the optimisation on our proposed robotic solution in order to find the optimal geometrical parameters which ensure an agreement between a compact mechanical structure and a sufficient workspace. The determination of this optimal configuration requires firstly the definition of a process (see Figure 4) which combines a modelling part and an optimisation part. The modelling step integrates a mathematical model for the geometric characterisation of the robot which is established in our case using the inverse geometric model introduced in Equation (1). This geometric information constitutes an input information for the optimisation part which is done over several steps. The parametrisation of the design must be elaborated by defining the geometric parameters of our robot which present here the parameters to be optimised. This step is essential since these geometric parameters are linked to the components of the robot and directly influence the objective function of the optimisation which will be identified later. They should be independent of each other as far as possible to reduce the complexity of the optimisation's implementation. In our case, at least seven basic geometric parameters are mandatory to define which present the length of the lower and upper frames L_1 and L_2, the radius of the base r and the mobile platform R and the angles θ_A, θ_c and θ_d taken into account to define the layout of the robot frames (see Figure 2). Thus, the vector of design parameters δ can be defined as follows:

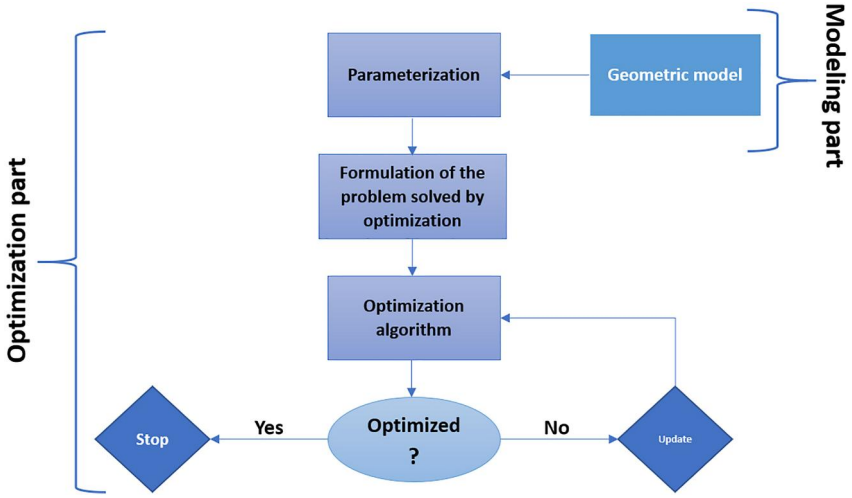

FIGURE 4 Optimisation process applied to our proposed robotic solution to determine the optimal design parameters

$$\delta = [r; R; L_1; L_2; \theta_A; \theta_c; \theta_d] \tag{18}$$

Then, the formulation of the problem to be solved by the optimisation is done by defining the constraints imposed on the joints and the components of the robot and also by defining the objective function. The physical constraints of the kinematic chain such as the limit of the rotary actuators should be considered. The rotary actuators have a specific range of work considered in Equation (19). These limitations are defined while rotating the lower frames of the robot in the CAD software without attending to the borders of the base and reaching singularities.

$$\theta_{\min} = 0^\circ < \theta_i < 90^\circ = \theta_{\max} \tag{19}$$

In addition, the constraints related to the dimensions of the design parameters were taken into account. Each one of them has a specific range of work to respect the limited size and weight of the robot imposed by the medical procedure requirements. These limitations allow having a compact and lightweight system able to be easily installed in the operating room with a size not exceeding the volume of a 300 mm edge cube. Table 2 shows the limitations of the vector δ considered in our study. After defining the constraints linked to the joints and the geometric parameters, the second step of the formulation of the problem solved by optimisation consists in defining the objective function. In our case, the objective of the optimisation is to ensure a sufficient workspace to allow the deposition of the radioactive seeds in the entire prostate's volume. For this, the objective function will be based mainly on the workspace determination since it presents the most important criterion in the LDR brachytherapy. The objective function, defined in Equation (20), compares the volume and workspace limits achievable for each set of geometric values ($V_{\text{workspace}}$) with the volume and workspace limits required for the LDR brachytherapy defined by V_r (equal to a free-singularities volume of 55 × 55 × 150 mm^3). This function gives a score adaptation between $V_{\text{workspace}}$ and V_r.

$$f(\delta) = \left\| V_{workspace}(\delta, \mathbf{X}) - V_r \right\| \tag{20}$$

To determine $V_{\text{workspace}}$, we implemented in MATLAB a recursive algorithm that determines the size and bounds of the robot's translation workspace for constant orientations ($\alpha = \beta = \gamma = 0°$). This computational algorithm integrates the discretisation method, which determines for specific values of the geometric parameters vector δ the inverse geometric model at each set of Cartesian coordinates. Once the inverse geometric model is solved and, the values of the rotary joints angles are determined, we check if these angles are within the range of rotary actuators constraints defined by Equation (19). In a case where the values of these angles respect these constraints, the Cartesian coordinates of the corresponding points will be saved, seeing that they define the operational workspace achievable by the robot's end-effector. Otherwise, these points will be discarded and excluded from the workspace.

In other words, the formulation of the problem solved by the optimisation can be resumed by the following scheme:

$$\begin{aligned} &\text{Find a vector } \delta = [r; R; L_1; L_2; \theta_A; \theta_c; \theta_d] \\ &\text{That Minimises : } f(\delta) \\ &\text{With keeping } 0^\circ < \theta_i < 90^\circ \\ &\text{and } \delta \in \textit{Table II} \end{aligned} \tag{21}$$

After the formulation of the problem solved by the optimisation, we move to the most crucial step that leads to the determination of the optimal geometrical parameters. This step consists of implementing the optimisation algorithm, which will be the genetic algorithm. We chose to work with this algorithm since its computation time is relatively reduced compared to other algorithms. In addition, this robust and powerful algorithm has better chances of obtaining the optimal solution.[25] It is inspired by the process of natural selection[26] and its operation principle is illustrated as follows. By analogy with our optimisation, the algorithm selects random values of the geometric parameters, defined by vector δ, from Table 2 while respecting maximum and minimum dimension values of each

parameter. Afterwards, it uses these random values to produce children of the next generation. In other words, from these randomly chosen geometric values, it produces for the following iteration another geometric values which obviously remain in the interval of the minimum and maximum values and make it possible to respect the objective function. The genetic algorithm uses three evolution operators each time to create future generations from current populations. These evolution operators are selection, crossing, and mutation; and they designate as follows:

- Selection: choice of the most suitable individuals.
- Crossover: mixing by reproducing the characteristics of the chosen individuals.
- Mutation: random alteration of the characteristics of an individual.

Thus, over the generations, the population evolves towards optimal solutions whose values are included in Table 2. We have created a code that involves the definition of the design parameters, the formulation of the problem to be solved, and the integration of a predefined module of the geometric algorithm in MATLAB.[27] This code allows the implementation of the optimisation algorithm and to search for the optimal values of the geometric parameters. The configuration of the parameters of the genetic algorithm adopted for our optimisation is presented in Table 3.

The solutions of our code implementation are obtained after a computation time of 1 day and 150 iterations using an Intel(R) Core (TM) i5-6500 CPU type processor. The stopping criterion of our algorithm is either exceeding the number of iterations defined initially, or obtaining the optimal solution. Indeed, several very close optimal solutions, whose objective function is the same, were found by the genetic algorithm. The geometrical parameters' solution of the robot chosen by the optimiser presents the average of the optimal solutions and is represented in Table 2. These parameters are applied to the CAD model of the robotic structure. We can see here that the overall dimensions of the robotic system can fill into a box of $300 \times 300 \times 300\ mm^3$, which satisfies the requirement of the LDR brachytherapy procedure. After calculating the theoretical volume of the robot using the discretisation method, we conclude that the end-effector can displace in a workspace superior to $55 \times 55 \times 150\ mm^3$ without encountering singularities.

6 | PROTOTYPE AND EXPERIMENTAL BENCH

The realisation of a primary prototype is necessary to practically evaluate the adequacy of the proposed solution with the requirements of LDR brachytherapy. We chose to build a prototype with the technique of 3D printing. To do that, we need to print each component apart by implementing its 3D model in 'Cura' software and then send it to the 3D printer 'Ultimaker S5'.[28] The final components, realised in black polylactic acid material, were assembled using several mechanical systems such as screw-nut and u-groove mechanisms.

TABLE 3 Configuration of the parameters of the genetic algorithm

Settings	Parameters of the genetic algorithm
350	Size of the population
Real	Coding type
Stochastic	Selection strategy
Dispersed	Crossing type
Adaptive	Mutation type
0.9	Crossing probability
0.1	Mutation probability

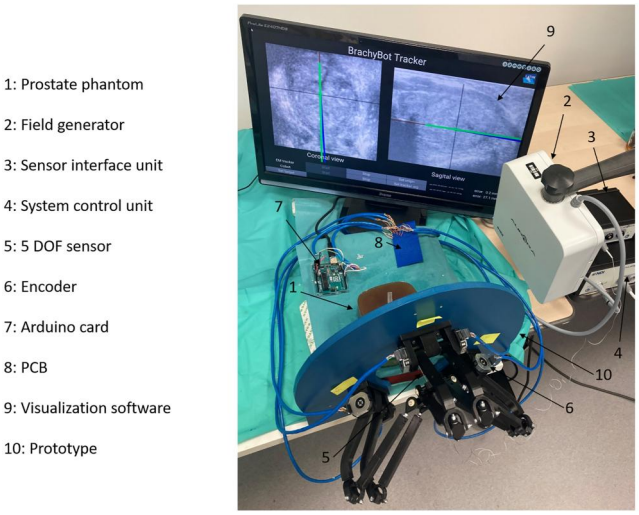

FIGURE 5 Experimental bench installed in our laboratory

This prototype was integrated to an experimental bench, established also in our laboratory, to define the protocol of the tests to be carried out. This experimental bench is shown in Figure 5 and is composed principally of: a prostate phantom, an electromagnetic (EM) tracker, electronic devices and a visualisation software. The prostate phantom (n°1) is a gelatinous structure that contains the different elements of the male reproductive system (prostate, urethra, rectum...). It is made from a mixture of thermoplastic polymer polyvinyl chloride and 1% of Psyllium to mimic the prostate tissues and reproduce some of the mechanical properties and ultrasound imaging of the organ.[13] This phantom will be placed parallel to the fixed platform of the prototype. As the control loop is still under development and not integrated into the robot yet, we choose using the EM tracker as an alternative measurement tool to validate the preliminary experiences. This latter is a system developed by Northern Digital Inc, Waterloo, Ontario, Canada[29] and is composed of: a field generator (n°2), a needle containing a 5-DOF sensor (n°5), a system control unit (n°4) and a sensor interface unit (n°3). These components work together to deliver the pose of the 18 G needle's tip attached to the end-effector of the robot. We note here that the 3D model of the end-effector was modified to adapt it to the measurement tool. The electronic devices group 6 modular absolute

AMT-203v encoders (n°6) that will be attached to the pivoting joints. They permit to determine the rotation angle of the pivoting joints by transmitting signals to an 'Arduino' card (n°7) and a printed circuit board (n°8) via the serial peripheral interface bus of communication. The visualisation software (n°9) was developed in our laboratory and had three main functions. The first is to extract the pose data of the needle's tip determined by the EM tracker. These data are displayed on a visualisation interface which shows the needle displacements (blue line on Figure 5) on a front view and side view. These two views correspond to the needle displacement in the sagittal and coronal plane of the prostate. The second function transfers the angular positions of each encoder via the serial port of the 'Arduino' to the computer and then use them as input variables to calculate the kinematics and determine the pose of the robot's end-effector. This pose is displayed on the same visualisation interface with the information transmitted by the EM tracker (green line on Figure 5). The calculation of the kinematics is done in loop to allow real-time display of the needle displacement on the visualisation interface. The third function allows the user to define a target and to calculate the error between this target and the pose of the needle.

Before establishing the experimental trials, we have to parameterise and set up the robotic system and the EM tracker to get all the measurement values in the fixed coordinate system R_0. For that, we attached a template grid (as the one presented by Figure 3) to the base of the robot, and we centred it relatively to the centre of R_0. Then, we placed the centre of the end-effector at point A of the template and we recorded the coordinates delivered by the EM tracker. These coordinates will be used in an inter-coordinate registration to get the pose of the different measurements realised with the EM tracker in R_0. Also, we placed the lower arms of the robot completely parallel to the fixed platform. After that, we created a code that allow us to define and set up the zero position of the encoders. This step is very important because it will permit getting the pose of the needle's tip, calculated by the kinematics, in R_0 as well.

7 | EXPERIMENTAL RESULTS

7.1 | Workspace measurements

The measurement of the workspace (translation and orientation) reachable by the end-effector presents an important step in the evaluation of the relevance of our prototype. Indeed, the robot must cover at least a translation workspace equal to $55 \times 55 \times 150$ mm^3 to reach all positions in the prostate. The theoretical study, done after the optimisation, has confirmed that our solution meets the specifications of LDR brachytherapy in terms of workspace. However, during this theoretical study, many constraints issues related to the medical application and the mechanical architecture could not be considered like the rotatory limits of the spherical and universal joints as well as the presence of the endorectal probe. We will measure the translation workspace of the robot for both cases (before and after integrating the ultrasound probe in the experimental bench) and we will compare the results with the theoretical calculation. To do that, we initially tried to displace the end-effector in all directions to the extremities of its reachable positions while avoiding singularities. Then, the coordinates of each of these positions are recorded with the EM tracker in a text file. Using these coordinates, the robot workspace is reconstructed with MATLAB and shown in the Figure 6. Here the transrectal ultrasound probe used is a 3D side-fire ultrasound probe of a frequency range of 4–9 MHz, a 146° field of view, and multiple imaging modes. It is characterised by 200 mm insertion length and 20 mm diameter. The volume of the reconstructed workspace without adding the probe is equal to 1800 cm^3 while it is equal to 1500 cm^3 when adding the probe. It corresponds respectively to 75% and 62% of the theoretical volume which is equal to 2400 cm^3. We can explain the difference between the experimental volumes and the theoretical one by the fact that we have not considered the mechanical constraints cited above and the risks of collision between the frames themselves and between the

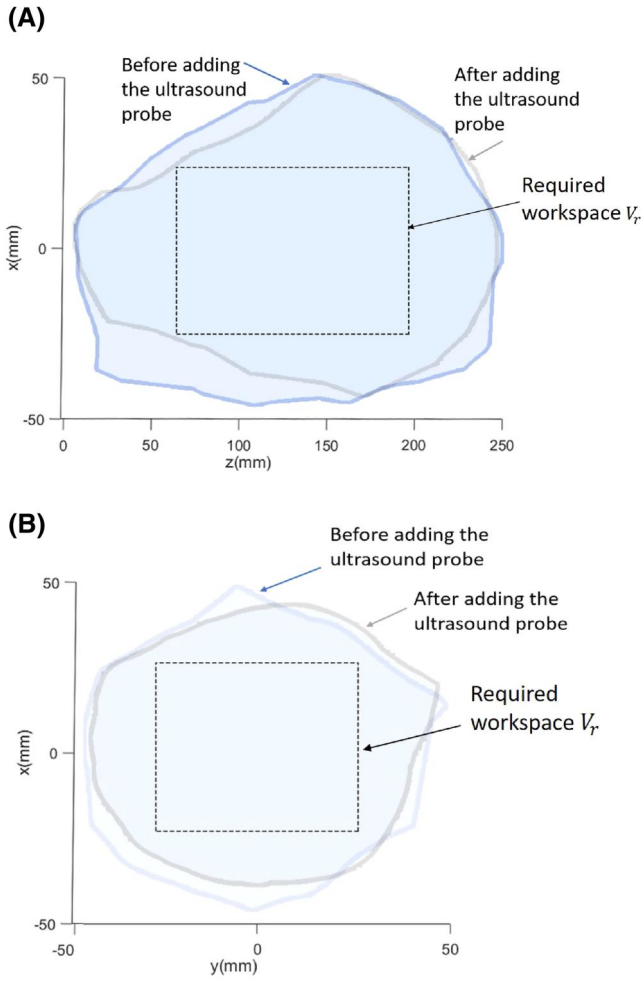

FIGURE 6 Results of the experimental measurements of the workspace before (blue zone) and after (grey zone) the addition of the ultrasound probe. The dotted shape corresponds to the volume required by the medical application. (A) *xz* plane, (B) *xy* plane

TABLE 4 Experimental results of the end-effector rotation around the three axes

End-effector rotation for different depth						Orientation errors		
z (mm)	250	180	120	60	10	5°	10°	15°
Roll: γ(°)	32	37	37	29	47	0.16	0.25	0.3
Yaw: β(°)	67	124	161	100	72	0.5	0.5	0.68
Pitch: α(°)	57	57	74	61	48	0.3	0.5	0.66

lower frames and the fixed platform. Comparing the experimental workspace reconstructed in the non-presence of the ultrasound probe with the one established in its presence, we find that it was slightly influenced by the addition of the probe, especially at the lower part (see Figure 6). In fact, when the ultrasound probe is introduced into the rectum of the phantom and is installed near the fixed platform, the displacement of the end-effector to reach configurations close to the base is limited. However, this does not affect the relevance of the mechanical design of our robot since, in the clinical context, the prostate of a patient installed in the lithotomy position is located in the upper part of the workspace. We can conclude that, in both cases, the end-effector covers the entire volume of the prostate without reaching singularity positions and/or being constrained by the elements present in the operating room.

To measure the orientation workspace, we first placed the end-effector at the base centre and we recorded the angular coordinates delivered by the EM tracker relative to this position. Afterwards, we measured the possible rotation around the 3 axes. As the rotation of the effector is dependent on several parameters (positions of the frames, collisions, rotatory limits of the spherical and universal joints, etc.), we tried to measure it for different positions along the axis of the needle insertion as shown on Table 4. The minimum experimental values corresponding to the angles of roll, pitch, and yaw are respectively 29°, 48°, and 67°. These results show that our robotic solution ensures pitch and yaw angles superior to 15° which corresponds to the required pitch and yaw angles for LDR brachytherapy. Consequently, the robot permits the surgeon to reach any position in the prostate and avoid interference with the pubic arch. Also, it allows sufficient rotation of the needle around its axis, which minimises the deformation of the needle during its insertion into tissues.

7.2 | Measurements of needle's tip errors by the robot kinematics

The intervention of LDR brachytherapy is done over two steps, the first consists of positioning the needle on the transperineal surface of the patient (with or without angulation), and the second consists in inserting it into the prostate. We must evaluate the kinematics of our robot and its ability to perform these two steps by performing measurements to determine the errors related to the positioning of the needles, its angulation around the three axes, and its insertion in the prostate phantom.

7.2.1 | Measurements of positioning errors

We chose point A as the centre of the robot coordinate system (see Figure 3) and saved the needle's pose delivered by the EM tracker to establish a reference change and to determine all the measurements relative to the robot coordinate system. After that, we manually positioned the needle on the point of the marking grid and we defined a target position using the visualisation software. For this target position, we stored the needle's pose delivered by the EM tracker. These last two operations are repeated for all the points of the marking grid (nine points). Finally, we tried to position again the needle on the phantom surface to reach the different target positions as before, but with the difference that here we noted the positioning error between the pose of the target measured by the EM tracker and that calculated via the encoders and the robot kinematics. We have presented in Figure 7 the target positions already defined using the visualisation software as entry points on the phantom and the positioning errors related to calculating the kinematics estimation. The average positioning error estimated by the kinematics is 2.4 mm. It can reach at best 1.1 mm and at worst 3 mm. We can remark from this experiment that the errors on the edges of the workspace are more important. This is caused by friction and 3D printing errors of the various components. Indeed, when the end-effector is moved to the limits of the positioning plane of the needle, the passive links of at least one pair of neighbouring frames are approximately in mechanical blocking. The theoretical results found by the calculation of the forward geometric model, show that the positioning error varies between 0.02 and 1.4 mm, and on average it is equal to 0.86 mm. This difference between the theoretical and experimental results is caused by several factors, principally, the limitations of 3D printing and the approximate calculation with the Newton-Raphson method. However, these results allow us to confirm that our robot is reliable for assisting the positioning of the needle on the transperineal surface since the errors are <3 mm and remain better than the errors of the conventional method.

7.2.2 | Measurements of insertion errors

We will repeat the experimental protocol established in the previous paragraph, except this time, we will calculate the needle placement errors for different depths in the prostate to mimic the insertion throughout the organ. To do this, for each entry point on the prostate puncture plane, we defined target positions at different depths spaced 10 mm apart. Then, we noted the errors indicated by the EM tracker and the estimation of the robot kinematics relative to the target positions (in the final, we did 63 measurements). In Figure 8, we have presented the insertion errors measured by the EM tracker (shown by green stars) and by the calculation of kinematics (shown by red squares) for the entry point A at different insertion depths. The insertion accuracy measured relatively to target positions reveals an average error of 0.73 and 0.78 mm for respectively the EM tracker and the robot kinematics estimation. These experimentally errors are caused by the deformation of the needle once it is inserted into the

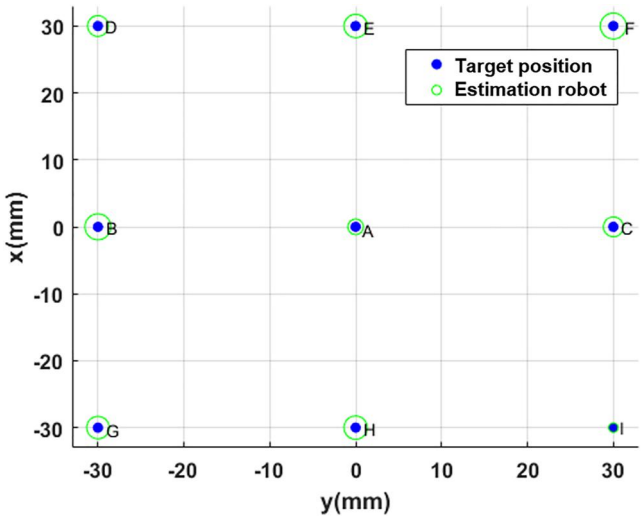

FIGURE 7 Positioning errors measured using the visualisation software between the target positions (points in blue) already predefined on the phantom surface and the poses determined by the calculation of the robot kinematics (circles in green)

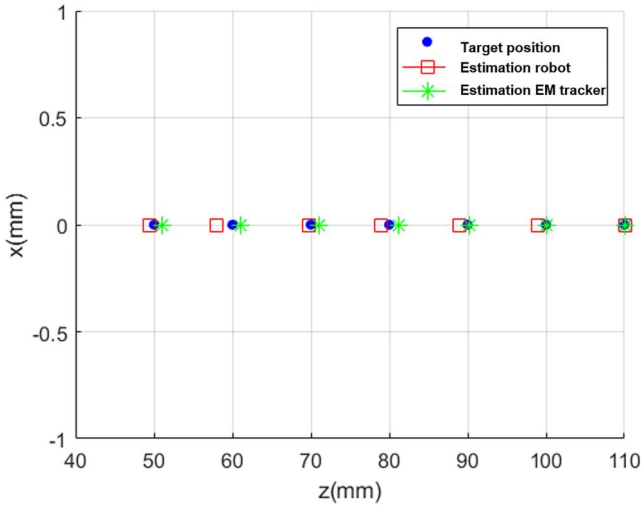

FIGURE 8 Insertion errors measured using the visualisation software, for point A, between the already predefined target positions (blue points) and the poses determined by the electromagnetic tracker (green stars) and by the calculation of kinematics (red squares)

prostate phantom. When the needle punctures the phantom, cutting forces will be applied to it which causes the deformation of its trajectory.

7.2.3 | Measurements of orientation errors

We positioned the needle's tip perpendicular to the entry points of the marking grid. Then, we revealed the angle values delivered by the EM tracker. These values will be used as initial values for the needle orientation around the three axes. Afterwards, we manually rotate the needle up to target angle values and we saved the error between these values and the values indicated by the kinematics estimation. This experiment is done for all entry points and target values of 5°, 10°, and 15° for pitch, yaw, and roll angle. The orientation errors represented in Table 4 vary between 0.16° and 0.66° and they are caused by the errors in estimating the needle's tip pose based on the angles delivered by the encoders.

TABLE 5 Average error calculated for all operators for each point of the marking grid

Points	A	B	C	D	E	F	G	H	I
Average errors (mm)	0.8	0.7	0.7	0.6	0.6	0.7	0.7	0.7	0.6

7.3 | Measurements of needle placement errors via visual feedback

The purpose of measuring the needle placement errors by the operator via visual feedback delivered by the visualisation software is to evaluate the capability of the robot to assist the surgeon in needle placement at the entry point and then its insertion into the phantom. As we haven't developed the robot control command at this stage, the only way is to use visual feedback. For this, we first fixed a marking grid on the surface of the phantom where we defined nine points (see Figure 3). This marking grid will help us define the limits of the region to be covered to position the needle's tip at several entry points on the phantom surface. Secondly, we inserted the needle to an arbitrary depth and defined a target position using the visualisation software. Then, we withdraw the needle and reinserted it to reach that target position only by the visual aid, and afterwards, we measured the needle placement error. This experiment was carried out by 14 operators (aged between 25 and 35 years old) and each operator repeats the same protocol for the nine entry points of the marking grid (we did in total 126 measurements).

According to Table 5, the average error varies between 0.628 and 0.807 mm and the overall average of all operators for the nine entry points is 0.7 mm. From these results, we can confirm that our robotic solution can assist the surgeon to place the seeds with a precision of <1 mm only by considering visual feedback via the current information of the needle in the prostate. Also, we find that there is not a significant difference between the different operators, which justifies that the robot can be used by a variety of people.

8 | DISCUSSION

The final robotic system is compact and lightweight providing ease of co-manipulation with the surgeons. It fits into a cube of $300 \times 300 \times 300$ mm^3 and ensures more than 15° orientation angles. It permits to reach any target position in a free-singularity workspace of $55 \times 55 \times 150$ mm^3. The proposed solution ensures 6-DOF which provides flexibility in displacing the needle and allows avoiding interference with the pubic arch. The average error between the measured position and the target position was 2.4 mm on the

positioning plane and 0.78 mm along the axis of needle insertion as well as the relative error of the angulation does not exceed 6%. The errors of accuracy are quite inferior to the conventional LDR brachytherapy which validates the added value of our proposed robotic system to the medical application. The theoretical and experimental studies show that our robot differs from the other robots developed in the literature and it can be an effective solution to solve the problems related to the use of robots for LDR brachytherapy. Indeed, one of its advantages is its reduced size compatible with the medical application requirements The experience, that measures the needle placement errors via visual feedback, proves the capability of our robot to assist the surgeons in placing the radioactive seeds.

To resume, the proposed robot is fully thought out for the LDR brachytherapy and it was designed to respect the medical application constraints. Its size was optimised to facilitate its installation on the operating room and allow it to be easily carried by the medical staff. With such a design the problem of cumbersomeness and bulkiness was resolved so that our robot can replace the manual conventional system, get rid of the use of the grid, and provide more mobility to the needle. Since the robot is designed to collaborate with the surgeon and will help him to place the radioactive seeds with precision, the medical application will become much easier and will not depend on the dexterity and experience of the surgeons. With an adaptive control loop, the robot is eligible to ameliorate the accuracy of the needle's tip placement and thus, a focalised and localised LDR brachytherapy will be achieved which will minimise the sexual and urinary side effects (incontinence, impotence, etc.) and reduce the risk of recurrence of the prostate cancer once it was treated.

Although the preliminary results seem promising; they also show that there are several limitations to be considered in future work to improve the performance of our robot and have a prototype that can be used in clinical trials. The first limitation is related to the installation of the motors on the fixed platform and the implementation of the control loop. As our robot is designed to co-work with the surgeon and guide him to the target position, the control loop must take into account the control in position as well as the control of the force exerted by the robot on its environment which depends on several factors (force of insertion in human tissues, the force of the surgeon in comanipulation, etc.) to ensure guidance by force feedback. In fact, during the medical intervention, the needle must be positioned on the transperineal surface and then inserted into the tissues to the target point in the organ therefore, the role of the control loop is to guide the surgeon to at the entry point and then during the insertion process. For that, a robust adaptive force control in the face of external variations (the influence of the human operator) can be a method to get guidance by force feedback. The second limitation is related to the errors obtained during the needle insertion into the prostate phantom. These errors are related to the cutting forces applied to the needle while the insertion process. When the needle crosses the phantom, reaction forces are created. These forces deform the needle and deviate its tip which may cause an error in placing the radioactive seeds in the target positions. The deviation of the needle's tip is not taken into account by the robot kinematics since it does not import relative changes of the pivoting joints' angle values. That's why mechanical modelling of the needle behaviour that can estimate the trajectory and deformation of the needle's tip has to be investigated and considered in the control loop for future work to take into consideration the variables stiffness and the cutting forces applied by the human tissues and thus compensate the interactive force change and minimise the needle deflection.[30]

In this study, we focussed on the LDR brachytherapy but there is another treatment which is called high-dose rate (HDR) brachytherapy and it is used also to treat early-stage prostate cancer. The HDR brachytherapy involves inserting thin tubes into the prostate gland. A high-dose radiation source is passed through these tubes until reaching the prostate for a few minutes to destroy cancer cells and then removed. Regardless of that this localised treatment significantly minimises side effects, it causes urinary and sexual disorders. Also, it requires to be carried out in a bunker for external irradiation where the patient is alone because this presents a danger for the medical staff. This intervention can be done one or more times which will be more painful for both the patient and the medical staff. There is not currently direct clinical evidence supporting the superiority of HDR or LDR brachytherapy concerning tumour control or reduced toxicity and the choice of the treatment depends on clinicians' preferences.[31] For that, many robots dedicated to HDR brachytherapy have been developed like the compact robot proposed by[32] where a study in human-centred automation that has the potential to reduce patient side effects from HDR brachytherapy has been presented. The design of our robot allows it to be used also for HDR brachytherapy since it is compact and it can be installed parallel to the operating table providing sufficient workspace to reach any target in the prostate. Some modifications should be done to the design of the end-effector to adapt it to carry out the thin tubes.

9 | CONCLUSION

In this paper, a parallel 6-DOF co-manipulated robot for LDR brachytherapy was presented and studied. It fulfils all the clinical design requirements and provides a beneficial alternative to the manual technique. The kinematics were investigated to simplify the study of the robot. An optimisation method was applied to find the optimal geometric dimensions that ensure an agreement between a sufficient workspace and a compact size. A prototype was created and experimental evaluations were established to practically measure the translation and orientation workspace and evaluate the errors in needle's tip placement.

ACKNOWLEDGEMENT

Authors would like to thank the Brest Regional University Hospital for providing them CT scans on prostate. This work was partly supported by the French Brittany Region.

CONFLICT OF INTEREST

All authors declared that they have no conflict of interests.

DATA AVAILABILITY STATEMENT

The data that support the findings of this study are available from the corresponding author upon reasonable request.

ORCID

Aziza Ben Halima https://orcid.org/0000-0002-6781-8662

REFERENCES

1. Skowronek J. Low-dose-rate or high-dose-rate brachytherapy in treatment of prostate cancer–between options. *J Contemp Brachytherapy*. 2013;5(1):33-41. https://doi.org/10.5114/jcb.2013.34342
2. Ferrer M, Suárez JF, Guedea F, et al. Health-related quality of life 2 years after treatment with radical prostatectomy, prostate brachytherapy, or external beam radiotherapy in patients with clinically localized prostate cancer. *Int J Radiat Oncol Biol Phys*. 2008;72(2):421-432.
3. Fu L, Liu H, Brasacchio R, et al. Clinical observation and modeling of postimplant seed displacement for prostate brachytherapy. *Int J Radiat Oncol Biol Phys*. 2005;63:S504-S505. https://doi.org/10.1016/j.ijrobp.2005.07.857
4. Taschereau R, Pouliot J, Roy J, Tremblay D. Seed misplacement and stabilizing needles in transperineal permanent prostate implants. *Radiother Oncol*. 2000;55(1):59-63. https://doi.org/10.1016/s0167-8140(00)00162-6
5. Podder TK, Beaulieu L, Caldwell B, et al. AAPM and GEC-ESTRO guidelines for image-guided robotic brachytherapy: report of Task Group 192. *Med Phys*. 2014;41(10):101501. https://doi.org/10.1118/1.4895013
6. Wei Z, Ding M, Downey D, Fenster A. 3d TRUS guided robot assisted prostate brachytherapy. In: *International Conference on Medical Image Computing and Computer-Assisted Intervention*. Springer; 2005:17-24.
7. Davies B, Harris S, Dibble E. Brachytherapy—an example of a urological minimally invasive robotic procedure. *Int J Med Robot Comput Assist Surg*. 2004;1(1):88-96. https://doi.org/10.1581/mrcas.2004.010108
8. Heikkilä V-P, Suorsa N. A technique for simultaneous needle insertion in prostate seed implantation. *Phys Med Biol*. 2008;53(4):N35-N39. https://doi.org/10.1088/0031-9155/53/4/n02
9. Hungr N, Troccaz J, Zemiti N, Tripodi N. Design of an ultrasound-guided robotic brachytherapy needle-insertion system. In: *2009 Annual International Conference of the IEEE Engineering in Medicine and Biology Society*. IEEE; 2009:250-253.
10. Bassan H, Hayes T, Patel RV, Moallem M. A novel manipulator for 3D ultrasound guided percutaneous needle insertion. In: *Proceedings 2007 IEEE International Conference on Robotics and Automation*. IEEE; 2007:617-622.
11. Fichtinger G, Fiene J, Kennedy CW, et al. Robotic assistance for ultrasound guided prostate brachytherapy. In: *International Conference on Medical Image Computing and Computer-Assisted Intervention*. Springer; 2007:119-127.
12. Dai X, Zhang Y, Jiang J, Li B. Image-guided robots for low dose rate prostate brachytherapy: perspectives on safety in design and use. *Int J Med Robot Comput Assist Surg*. 2021;17(3):e2239. https://doi.org/10.1002/rcs.2239
13. Djohossou M, Halima AB, Valérie A, Bert J, Visvikis D. Design and kinematics of a comanipulated robot dedicated to prostate brachytherapy. *Robotica*: 1-15.
14. Gibbons EP, Smith RP, Beriwal S, Krishna K, Benoit RM. Overcoming pubic arch interference with free-hand needle placement in men undergoing prostate brachytherapy. *Brachytherapy*. 2009;8(1):74-78. https://doi.org/10.1016/j.brachy.2008.04.007
15. Halima AB, Bert J, Clément J-F, Visvikis D. Development of a 6 degrees of freedom prostate brachytherapy robot with integrated gravity compensation system. In: *2021 International Symposium on Medical Robotics (ISMR)*. IEEE; 2021:1-7.
16. Zhang S-J, Qian H-N, Zhao Y, et al. Relationship between age and prostate size. *Asian J Androl*. 2013;15(1):116-120. https://doi.org/10.1038/aja.2012.127
17. Hall TL, Hempel CR, Sabb BJ, Roberts WW. Acoustic access to the prostate for extracorporeal ultrasound ablation. *J Endourol*. 2010;24(11):1875-1881. https://doi.org/10.1089/end.2009.0567
18. Fischer GS, Iordachita I, DiMaio SP, Fichtinger G. Design of a robot for transperineal prostate needle placement in MRI scanner. In: *2006 IEEE International Conference on Mechatronics*. IEEE; 2006:592-597.
19. Hunt KH, Structural kinematics of in-parallel-actuated robot-arms. 1983.
20. Gosselin C, Angeles J. Singularity analysis of closed-loop kinematic chains. *IEEE Trans Robot Autom*. 1990;6(3):281-290. https://doi.org/10.1109/70.56660
21. Zabalza I, Pintor J, Ros J, Jimenez J. Evaluation of the 64 'insensitivity' positions for a 6-RKS hunt-type parallel manipulator. In: *Proceeding of the Tenth World Congress on the Theory of Machine and Mechanisms*. 1999:20-24.
22. Neto CSF, Schutel C. Orientation workspace optimization for a 6-RUS parallel robot. In: *ABCM Symposium Series in Mechatronics*. Vol. 6. 2014.
23. Joumah AA, Albitar C. Design optimization of 6-RUS parallel manipulator using hybrid algorithm. *Int J Inf Technol Comput Sci*. 2018;10(2):83-95. https://doi.org/10.5815/ijitcs.2018.02.08
24. Taherifar A, Najafi E, Nahvi A, Najafi F. Kinematic optimization of stewart platform for simulators using genetic algorithm. In: *6th annual IEEE Conference on Automation Science and Engineering*; 2013:123-129.
25. Kramer O. Genetic algorithms. In: *Genetic algorithm essentials*. Springer; 2017:11-19.
26. Genetic algorithm. 2021. Page Version ID: 1029032850. [Online]. Accessed June 29, 2021. https://en.wikipedia.org/wiki/Genetic_algorithm
27. Find minimum of function using genetic algorithm - MATLAB ga. [Online]. Accessed June 13, 2022. https://www.mathworks.com/help/gads/ga.html
28. Ultimaker Cura: un logiciel d'impression 3D puissant et facile à utiliser. [Online]. Accessed June 10, 2022. https://ultimaker.com/fr/software/ultimaker-cura
29. NDI - electromagnetic tracking & optical measurement solutions. [Online]. Accessed June 29, 2021. https://www.ndigital.com/
30. Li Y, Yang C, Bahl A, Persad R, Melhuish C. A review on the techniques used in prostate brachytherapy. *Cognit Comput Syst*. 2022. https://doi.org/10.1049/ccs2.12067
31. Gray C, Campbell K. High dose rate brachytherapy versus low dose rate brachytherapy for the treatment of prostate cancer: a review of clinical effectiveness and cost-effectiveness. Canadian Agency for Drugs and Technologies in Health; 2019.
32. Garg A, Siauw T, Berenson D, et al. Robot-guided open-loop insertion of skew-line needle arrangements for high dose rate brachytherapy. *IEEE Trans Autom Sci Eng*. 2013;10(4):948-956. https://doi.org/10.1109/tase.2013.2276940

How to cite this article: Ben Halima A, Bert J, Clément J-F, Visvikis D. Optimisation and validation of a co-manipulated robot for brachytherapy procedure. *Int J Med Robot*. 2023;19(1):e2465. https://doi.org/10.1002/rcs.2465